

# Sensor Architecture for a Two-Actuator Robotic Endoscope Tip

Yi Chen, Jillian M. Oliveira, and Ian W. Hunter

**Abstract**—An angular positioning methodology for a two-actuator robotic endoscope tip is presented. The actuators used to position the tip of the endoscope and tools in the tool channel are miniature rotary motors configured to pull mono-filament cables. The sensors used in this system are a camera at the tip and two three-axis gyroscopes. This paper discusses the electrical hardware and communications architecture of the system. A model to account for the dynamic nonlinearities in the system is introduced, experimental results are presented, and control schemes necessary to position the tip is outlined. It was found that the maximum rotational speed of the tip is 400 degrees per second and that the windup delay is around 50 ms which allows for fast angular positioning.

## I. INTRODUCTION

As tools, sensors, and requirements for many visual diagnostic and minimally invasive medical procedures become more complex, the basic endoscope platform used as the workhorse for these procedures also needs to evolve. Endoscopes have not only been used for traditional colonoscopies but have been adapted for use in natural orifice transluminal endoscopic surgery (NOTES) [1], minimally invasive surgeries such as pericardioscopy [2], [3], and several other novel procedures [4]. Each of these procedures requires (or can benefit from) assisted tool positioning, closed-loop position control, feature tracking and image stabilization, built-in force limits, and haptic feedback.

Cauterization, ablation, and biopsy instruments are some of the most common tools used in conjunction with an endoscope. It is important to get these tools, along with the endoscope camera, to the location of interest and be able to position the tool as well as the camera. Many endoscopic procedures require the attention of several doctors and nurses to manipulate the multitude of tools. With closed loop position control, feature tracking and image stabilization [4], some of the medical professionals can be free to manipulate other instruments while the endoscope maintains the view of the camera or the location of one of the tools. This can lessen the cost and reduce the complexity of procedures. Unintentional perforations in the viscera can occur during endoscopic procedures due to excessive forces applied at the endoscope tip [5], [6]. With Bowden cable actuation approaches, where the cables that turn the tip of the endoscope extend along the entire length of the endoscope, the force applied at the tip of endoscope depends heavily on the number of turns that

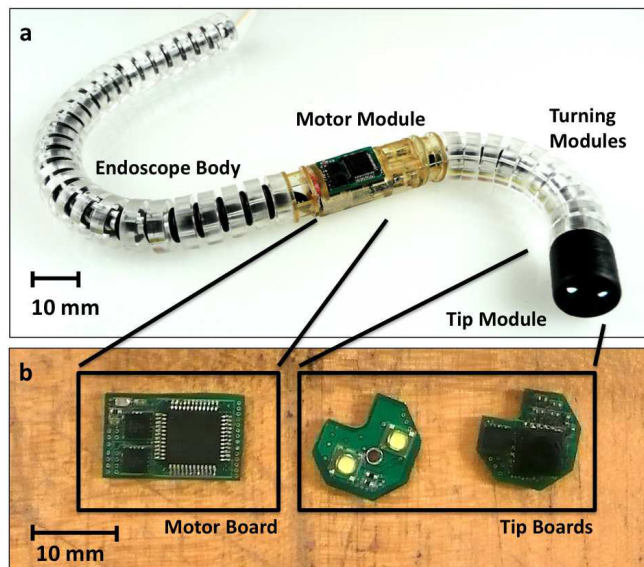


Fig. 1. a) Endoscope tip showing the tip module, the turning modules, and the motor modules with the outer sheath removed (15 mm OD). The tool passage, passages for wiring, fluid passages are also visible. b) Electronic boards that are located at the tip (including a camera, gyroscope, microprocessor, and lights) and located at the motor module (including microprocessor, gyroscope, and motor drivers) are shown.

occur in the length. With tip actuation approaches [3], [5], [7], it is much easier to control the forces applied at the tip to eliminate unintentional damage to tissue. Haptic feedback is also an important part of manual endoscope manipulation. Introducing haptic feedback can help decrease procedure time, make positioning more intuitive thereby increasing acceptance, and reduce the number perforations [8].

This paper presents the electronic architecture for an endoscopic robotic platform that incorporates these features, as shown in Fig. 1. A two-dimensional model of the tip actuation with dynamic nonlinearities is presented along with experimental results which illustrate some of the capabilities of the system. The design is meant to be low-cost so that the platform can be applied to single-use applications, which can alleviate cross-contamination, decrease chemical colitis, eliminate damage caused by wear-and-tear, reduce the cost, decrease the time necessary for cleaning endoscopes, and curtail the incidence of related hospital visits [5], [6].

## II. DESIGN ARCHITECTURE

The mechanical architecture for the single-use system includes motor modules, geared rotary motors, mono-filament control cables attached to a rotary-to-linear transmission,

Manuscript received June 20, 2011 for the IEEE EMB Conference  
Y. Chen, J. M. Oliveira and I. W. Hunter are with the Mechanical Engineering Department, Massachusetts Institute of Technology, Cambridge, MA, U. S. A. (contact: yichen@mit.edu)

turning modules, and a tip module that houses the camera and sensors [5]. The instrument shown in Fig. 1 differs from previous work in that the two motors which control x- and y-axis angular motion are colocated in the same module. Tip actuation with a geared rotary motor has advantages over shape memory alloys [4], [9], pneumatic [10], [11], and lead screw [12] options because of a combination of higher speed, lower cost, and greater compactness of the actuator and accessories. Since this design is modular, different modules, such as a more powerful rotary-to-linear transmission design, can easily be swapped to achieve higher pulling forces.

The single use components, which encompasses all the components which enter the body during the procedure including the motor, turning, and tip modules, are designed to be modular to reduce cost. At high volumes, the cost of the motors, electronics, and other components scales with readily available consumer devices such as disposable prepaid cell phones. Since these components are single-use, they only need to be sterilized once during initial commissioning. The sensors and actuator architecture including circuit boards, primary sensors and actuators are shown in Fig. 2.

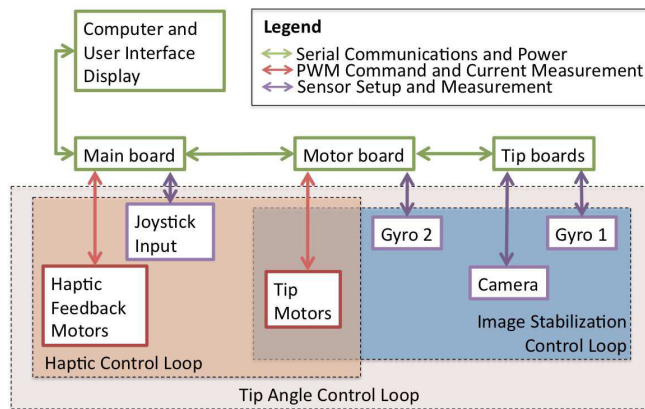


Fig. 2. Sensors and actuator architecture including electronic circuit boards, motors, a joystick input, gyroscopes and a camera. The image stabilization control loop, the haptic control loop and the main tip angle control loop along with associated sensors and actuators are outlined.

This distributed modular architecture has several benefits. First, the modular architecture provides distributed computing resources which enables dedicated local calculations (image acquisition and sensor integration). Second, it greatly reduces the number of wires that need to be passed through the body of the endoscope which reduces the stiffness of the system. Lastly, a modular architecture allows for a simple interface between the single-use components and the permanent components.

The layout includes electronics that are located inside the single-use endoscope and more complex electronics that are located in a permanent housing which is attached to a computer and a user interface display. The permanent electronics on the main board includes the user input joystick and haptic feedback motors as well as an Arm Cortex M3

microprocessor which interfaces with the computer using USB. In order to keep the layout modular, the main board interfaces with the single-use endoscope electronics via a synchronous serial peripheral interface bus.

The motor board which lays horizontally along the motor module, houses a smaller form factor Cortex M3 microprocessor which commands motor drivers in PWM mode and measures motor current to control the two actuation motors. The board also houses a three-axis gyroscope (InvenSense ITG-3200) which is used to determine the turning angle of the tip. The motor board interfaces with the tip board via a second synchronous serial peripheral interface bus. The tip board includes a VGA camera (Toshiba TCM8230MD) which can communicate through 8-wire parallel lines with a smaller form factor Cortex M3 microprocessor. It also has an extension board with two white LED lights with luminous power of 120 lm or more.

The tip boards, which are under 12 mm in diameter and contain a notch for a tool passage, houses a second three-axis gyroscope; two gyroscopes are necessary for determining relative angle between the motor module and the tip module. The gyroscopes are used to implement accurate blind turns (turns that may be outside the field of view of the camera) and to provide higher speed responses to angle perturbations than the camera and image processing algorithm is able to output. Because of possible drift, the gyroscope integration and calibration is done on the local board and the gyroscope is only used for relative turns.

Three major control loops that are used to drive the system are also shown in Fig. 2. The large outer control loop includes all the sensors and actuators. This control loop takes inputs from the joystick and sends angle commands to the tip motors using the gyroscopes for accurate closed loop turns. In this loop, the user can utilize the camera to determine positioning or can request blind turns. The next loop is the image stabilization control loop which includes the gyroscopes, the camera, and the tip motors. This loop processes the images from the camera to determine the movements necessary to keep an object of interest in the center of the image. The gyro readings are used for the closed loop control and the camera information is used as the input command. The final control loop is for the haptic system which measures the motor output torque and translates it to a resistance on the joystick to indicate to the user the amount of force being applied at the tip. The sensor interfaces and control algorithms are written in embedded C and assembly languages for speed.

### III. MODEL

This modular motorized design has several interesting features that must be considered for controls including inaccessible angular locations, nonlinearities in the drive dynamics, and windup delay when reversing inputs. With one motor pulling in the x-axis and one pulling in the y-

axis, it is not possible to access all possible angles if the x- and y- axes are limited to  $\pm 180^\circ$ . In addition, a single motor per axis with a simple linear to rotary transmission inherently has one taut cable and one loose cable which causes windup delay when reversing directions. Furthermore, the friction and backlash in the gearing will cause a deadband at low input voltages.

The deadband nonlinearity and the input limit nonlinearity in the x (or y) direction can be modeled as,

$$V_{inx} = \begin{cases} \text{sgn}(V_x)V_{max} & \text{if } |V_x| < V_{min}, \\ V_x & \text{if } |V_x| \geq V_{min}, \\ 0 & \text{otherwise,} \end{cases} \quad (1)$$

where  $V_x$  is the input voltage,  $V_{min}$  is the minimum voltage necessary to overcome static frictional losses in the system, and  $V_{max}$  is the maximum allowable input voltage to the motor.

The windup delay nonlinearity can also be modeled. If the input command is proceeding in a one direction (grouped by  $V_{inx} > 0$  or  $V_{inx} < 0$ ) then the dynamic equation for angular movement in a single axis can be derived from a force balance, torque balance, and by accounting for capstan friction [5] using

$$J\ddot{x} + B\dot{x} + Kx - \frac{L_h - L_s}{r(D_m + D_s)} T_{in} e^{-\mu(x + \frac{\pi}{2})} = 0, \quad (2)$$

$$T_{in} = \frac{NK_t}{R} \left( V_{inx} - \frac{K_e n (L_h - L_s)}{rNn} \cos(x/n) \dot{x} \right), \quad (3)$$

where  $J$ ,  $B$ , and  $K$  describe the inertial, damping and spring constants,  $L_h$  is distance of the pull string from the center of the turning module,  $L_s$  is the radius of the spacer between the turning modules,  $D_m$  is the height of a turning module,  $D_s$  is the height of the spacer,  $r$  is the radius of the torque transmission shaft, and  $\mu$  is the coefficient of friction. The maximum angular limit is  $x_{max} = 2n \sin^{-1} \left( \frac{D_s}{2(L_m - L_s)} \right)$  where  $L_m$  is the radius of the turning module. The input torque  $T_{in}$  is a function of  $R$  which is the resistance of the motor,  $K_t$  and  $K_e$  which are the motor constants,  $N$  which is the motor gear ratio, and  $n$  which is the number of turning modules. While one cable of length  $s_{x1}$  is taut, the opposing cable of length  $s_{x2}$  becomes looser which can be described as

$$s_{x1} = d - L_h x - nK_c D_s x, \quad (4)$$

$$s_{x2} = d + L_h x + nK_c D_s x, \quad (5)$$

where  $d$  is the length of the turning module section, and  $K_c$  is the compression of each of the spacers.

When the motor change directions (from  $V_{inx} > 0$  to  $V_{inx} < 0$  or vice versa), the motor simply winds up the loose cable, the tip angle is preserved and all derivatives are set to zero ( $\dot{x} = x$ ,  $\dot{x} = 0$ ,  $\ddot{x} = 0$ ). The windup speed  $\frac{ds_x}{dt}$  is a function of input voltage such that

$$\frac{ds_x}{dt} = \frac{rN}{K_e} V_{inx}. \quad (6)$$

In the condition that the cable is taut ( $s_x = d + L_h x$ ), we return to solving the single-sided dynamic Eqns. 2 and 3. These equations can then be used to predict the behavior of the robotic endoscope and can be used to guide in controller design.

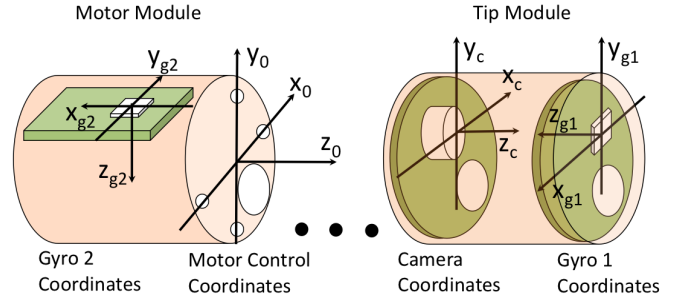


Fig. 3. Local coordinate systems for the gyroscope at the motor module, the gyroscope at the tip module, the camera, and the motor control location on the motor module. The ellipsis indicates that the relative coordinates between the motor module and tip module are unconnected.

To translate sensor readings into control inputs, it is important to translate the information in a given sensor's frame of reference to the motor control frame of reference. Figure 3 indicates the nominal alignment of each sensor relative to the motor module control coordinate system. Each of these coordinate systems needs to be translated back to the motor control frame of reference and mapped to an appropriate sensor reading in the x-rotational frame and the y-rotational frame which correspond to the two turning motors,

$$x_i^* = \cos(\beta_i) \cos(\gamma_i) x_i - \cos(\beta_i) \sin(\gamma_i) y_i + \sin(\beta_i) z_i, \quad (7)$$

$$y_i^* = [\cos(\alpha_i) \sin(\gamma_i) + \sin(\alpha_i) \sin(\beta_i) \cos(\gamma_i)] x_i + [\cos(\alpha_i) \cos(\gamma_i) - \sin(\alpha_i) \sin(\beta_i) \sin(\gamma_i)] y_i - \sin(\alpha_i) \cos(\beta_i) z_i, \quad (8)$$

where  $x_i$ ,  $y_i$  and  $z_i$  are the rotational rate outputs (radians/s) or integrated rotational angle outputs (radians) of the sensors and  $x_i^*$  and  $y_i^*$  are the desired readings used by the controller. The counterclockwise rotation angles  $\alpha_i$ ,  $\beta_i$  and  $\gamma_i$ , which are along the x, y and z axes respectively, are nominally  $\alpha_{g1} = 0^\circ$ ,  $\beta_{g1} = 180^\circ$  and  $\gamma_{g1} = 0^\circ$  for the tip gyroscope and  $\alpha_{g2} = 90^\circ$ ,  $\beta_{g2} = 0^\circ$  and  $\gamma_{g2} = -90^\circ$  for the gyroscope in the motor module when calibrated to zero while the motor module and the tip modules are aligned.

For the camera, the rotational outputs for tracking objects or for tracking relative motion can be approximated for small rotations as  $\Delta x_c = \frac{p_x}{t_x} f_x$  where  $p_x$  is the displacement in the x-direction measured in pixels,  $t_x$  is the total number of pixels in the x-direction, and  $f_x$  is the field of view of the camera in the x-direction measured in degrees. A similar equation can be determined for  $\Delta y_c$ .

#### IV. RESULTS

In order to validate the model, experiments were conducted on the gyroscope control loop since this is the primary controller that is used by the tip angle and image stabilization loops. The measured and simulated results on a 12 mm OD device with a gain-scheduled proportional and derivative control scheme involving blind (unaided by the camera) turns of  $\pm 45^\circ$  is shown in Fig. 4. Gain scheduling is necessary to overcome frictional forces and other nonlinearities. The



gyroscopes periodically report the results to the user interface which is shown in red.

Despite the deadband and windup delay nonlinearities, the maximum angular rotation rate for this design is around 400 degrees per second. The windup delay at  $45^\circ$  is about 50 ms which is smaller than the delay caused by inertia and friction which can be seen in the figure. Fortunately, due to the nonlinear nature of the dynamic Eqns. 2 and 3, the endoscope tip comes to an abrupt stop when the motor input is removed, sometimes overshooting slightly due to inertia. In contrast to linear systems and controllers, the nonlinearities in this system cause the endoscope tip to arrive quickly and stop abruptly at its destination with minimal oscillation.

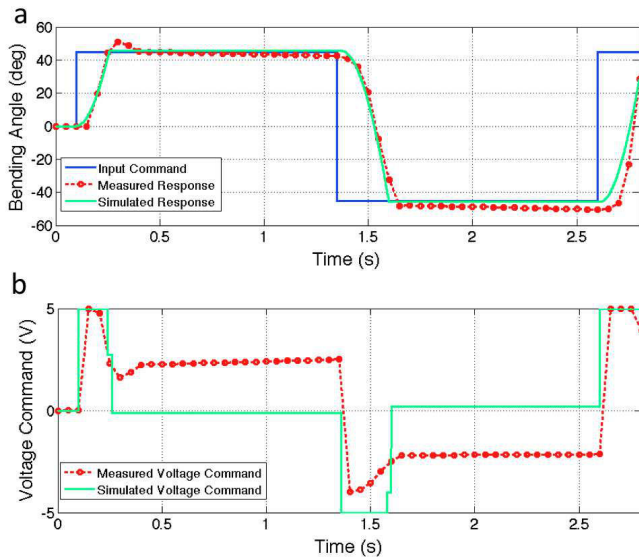


Fig. 4. a) The measured and simulated bending angle in the motor control frame of reference on the x-axis for a given input command. b) The voltage command from the controller showing the measured and simulated values. Simulation and experiment were completed on a 12 mm OD prototype.

Figure 4b shows the voltage commands sent to the motors. The motor inputs, which are hard limited to between  $\pm 5$  V, show matching patterns for the command structure. The overall trend, however, differs because the experimental system compensates for sensor drift, noise, and friction.

## V. CONCLUSION

The electronics, communications and sensor architecture presented in this paper helps to further the development of a single-use, robotic endoscope. The design is modular, utilizing several microprocessors at different critical locations. The device uses two gyroscopes for fast relative angle positioning and processed image data for lower speed object tracking. A model which accounts for several of the nonlinear dynamics of the system, including deadband nonlinearities, windup delay nonlinearities, and geometric nonlinearities was presented to help guide in the design of control algorithms. Closed-loop control was then demonstrated for this system with matching predictions from the model.

Future work on this platform would be to test the system in a clinical environment, to determine the proper user interface and to assess performance in the intended environment. This unique sensor architecture and controller framework may lead to future applications of robotics in medical devices.

## VI. ACKNOWLEDGMENTS

The authors acknowledge Shigehiko Tanaka and Al Couvillon for their previous work on the project. The authors would also like to thank Dr. Brian Hemond, Bryan Ruddy, and Dr. Cathy Hogan for their assistance. The project partially was supported by the Department of Defense (DoD) through the National Defense Science & Engineering Graduate Fellowship (NDSEG) Program, 32 CFR 168a.

## REFERENCES

- [1] S. J. Phee, S. C. Low, V. A. Huynh, A. P. Kencana, Z. L. Sun, and K. Yang, "Master and slave transluminal endoscopic robot (MASTER) for natural orifice transluminal endoscopic surgery (NOTES)," in *31st Annual International Conference of the IEEE Engineering in Medicine and Biology Society*, pp. 1192–1195, 2009.
- [2] G. Manca, R. Codecasa, A. Valeri, L. Braconi, G. Giunti, A. Tedone, A. M. Perna, P. Stefano, and G. Gensini, "Totally endoscopic subxiphoid pericardioscopy: early steps with a new surgical tool," *Surgical Endoscopy*, vol. 12, pp. 444–446, 2009.
- [3] F. Cepolina and R. C. Micheline, "Review of robotic fixtures for minimally invasive surgery," *International Journal of Medical Robotics and Computer Assisted Surgery*, vol. 1, no. 1, pp. 43–63, 2004.
- [4] J. M. Stevens and G. D. Buckner, "Actuation and control strategies for miniature robotic surgical systems," *Dynamic Systems, Measurement, and Control*, vol. 127, pp. 537–549, 2005.
- [5] Y. Chen, S. Tanaka, and I. W. Hunter, "Disposable endoscope tip actuation and robotic platform," in *32nd Annual International Conference of the IEEE Engineering in Medicine and Biology Society*, pp. 2279–2282, 2010.
- [6] D. A. Leffler, R. Kheraj, S. Garud, N. Neeman, L. A. Nathanson, C. P. Kelly, M. Sawhney, B. Landon, R. Doyle, S. Rosenberg, and M. Aronson, "The incidence and cost of unexpected hospital use after scheduled outpatient endoscopy," *Archives of Internal Medicine*, vol. 170, no. 19, pp. 1752–1757, 2010.
- [7] J. Peirs, D. Reynaerts, and H. Van Brussel, "A miniature manipulator for integration in a self-propelling endoscope," *Sensors and Actuators A*, vol. 92, pp. 343–349, 2001.
- [8] B. T. Bethea, A. M. Okamura, M. Kitagawa, T. P. Fitton, S. M. Cattaneo, V. L. Gott, W. A. Baumgartner, and D. D. Yuh, "Application of haptic feedback to robotic surgery," *Journal of Laparoendoscopic & Advanced Surgical Techniques*, vol. 14, no. 3, pp. 191–195, 2004.
- [9] J. Peirs, D. Reynaerts, and H. Van Brussel, "Design of a shape memory actuated endoscope tip," *Sensors and Actuators A*, vol. 70, pp. 135–140, 1998.
- [10] A. Menciassi, J. H. Park, S. Lee, S. Gorini, P. Dario, and J. Park, "Robotic solutions and mechanisms for a semi-autonomous endoscope," in *Proceedings of the International Conference on Intelligent Robots and Systems*, pp. 1379–1384, 2002.
- [11] D. Glozman, N. Hassidov, M. Senesh, and M. Shoham, "A self-propelled inflatable earthworm-like endoscope actuated by single supply line," *IEEE Transactions on Biomedical Engineering*, vol. 57, no. 6, pp. 1264–1272, 2010.
- [12] H. Ueno, Y. Ikeda, T. Sato, and S. Nakamura, "Endoscope," U. S. Patent 7,780,593 Aug 24, 2010.